MODELING CARDIAC CELL BIOPHYSICS USING LONG-SHORT-TERM MEMORY NETWORKS

Bruna Gonçalves

Graduate Student
Norfolk State University
700 Park Avenue
Norfolk, VA, USA
b.s.goncalves@spartans.nsu.edu

Makarand Deo

Department of Engineering
Norfolk State University
700 Park Avenue
Norfolk, VA, USA
mdeo@nsu.edu

ABSTRACT

Human induced pluripotent stem cell-derived cardiomyocytes (hiPSC-CMs) are being used to investigate mechanisms of various life-threatening cardiac disorders and drug effects. Long Short-Term Memory (LSTM) is a type of artificial neural network that has become popular for finding patterns from previous time steps to help predict the future response. In this paper, we developed LSTM-based predictive models to represent the electrophysiological response of a typical hiPSC-CM. Our model is able to reproduce experimentally observed effects on the action potential (AP) morphology for alterations in 5 main ionic currents in hiPSC-CMs. The proposed model achieved an impressive accuracy of 98.5% when compared to a detailed mathematical model of hiPSC-CM based on AP duration parameters (APD_{50}, APD_{75}, APD_{90}). The proposed approach has the potential to reduce the computational time of multiscale cardiac electrophysiology simulations and can be used in mechanistic studies to investigate inherited arrhythmia syndromes and patient-specific drug therapies.

Keywords: Deep Learning, stem cell-derived cardiomyocytes, Long Short-Term Memory (LSTM), cardiac electrophysiology modeling.

1 INTRODUCTION

Engineering strategies to use stem cells in biological research are among the breakthrough biological discoveries of the 21st century. Stem cells have a remarkable potential to differentiate into many cell types, and with recent advances in cell differentiation techniques, they may provide a viable alternative to specific human cell types such as nerve cells, kidney cells, cardiac myocytes etc. Human Induced Pluripotent Stem Cells (hiPSCs) are a class of stem cells derived from specialized somatic cells that have been reprogrammed to become pluripotent. hiPSC-derived cardiomyocytes (hiPSC-CMs) have recently been used successfully in studying cardiac safety pharmacology and various inherited and acquired cardiac arrhythmia disorders (Moretti et al. 2010). The Comprehensive *in vitro* Proarrhythmia Assay (CiPA) initiative stipulates research directions around the use of hiPSC-CM experimental data and mathematical modeling in proarrhythmic risk assessment (Colatsky et al. 2016).

Accurate numerical biophysical models can be employed to elucidate mechanisms of cardiac rhythm disorders and their clinical implications. The predictive modeling has been increasingly used to investigate the missing link between experimental observations and clinical translation. Recently, Akwaboah et al. (Akwaboah et al. 2021) formulated a detailed model of hiPSC-CMs based on extensive experimental data which is able to accurately reproduce the biophysical dynamics of hiPSC-CMs. The model consists of ionic current formulations of 14 key channels, pumps, and exchangers, along with intracellular calcium

homeostasis. The model was used to provide insights into the causes of the experimentally observed suppression of automaticity in hiPSC-CMs during cholinergic stimulation.

The movement of various ions, such as sodium (Na^+), potassium (K^+) and Calcium (Ca^{2+}), across the cell membrane through voltage gated channels gives rise to changes in transmembrane voltage (V_m), called action potential (AP). A typical AP of cardiac myocyte consists of five phases. 1) Phase 0, a resting phase, where the membrane potential is almost steady in the range of -60mV to -80mV. Inward rectifier potassium current (I_{K1}) and pacemaker current (I_f) play major roles in this phase. 2) Phase 1, a rapid depolarization phase resulting from fast sodium current (I_{Na}) occurring at suprathreshold voltage conditions. 3) Phase 2, a brief repolarization resulting from transient outward potassium current (I_{to}). 4) Phase 3, a plateau formed from a contention between inward L-type calcium current (I_{CaL}) and ultra-rapid delayed rectifier potassium current (I_{kur}). 5) Phase 4, a rapid repolarization phase dominated mostly by rapid delayed rectifier potassium current (I_{kr}). Figure 1 shows a typical AP of hiPSC-CM and key currents responsible in each phase.

From a modeling perspective, the AP is a process that needs information from the past and present states to predict the future behavior, known as a time series. In recent decades, deep Artificial Neural Networks (ANNs) have captured the world's attention by offering novel solutions to complex modeling of time series. Recurrent Neural Networks (RNNs) and LSTMs are classes of neural networks that have gained popularity in handling time series data (Han et al. 2021; Weerakody et al. 2021). RNNs contain gates which are activated at each time step, allowing information to be stored for the next time step in order to provide a temporal memory property. However, these gates are not capable of storing long-term information. To resolve this problem, Hochreiter and Schmidhuber (Hochreiter and Schmidhuber 1997) developed the LSTM algorithm as a modification to RNN (Pascanu et al. 2013) that is able to retain valuable information for long term, which is essential for non-linear times series prediction (Peter and Matskevichus 2019).

In this study, we propose an LSTM model as an alternative to traditional ODE solvers to drastically reduce the number of computations and simulation time involving hiPSC-CM biophysics. We utilized two different LSTM architectures to compare the performance of AP time series prediction.

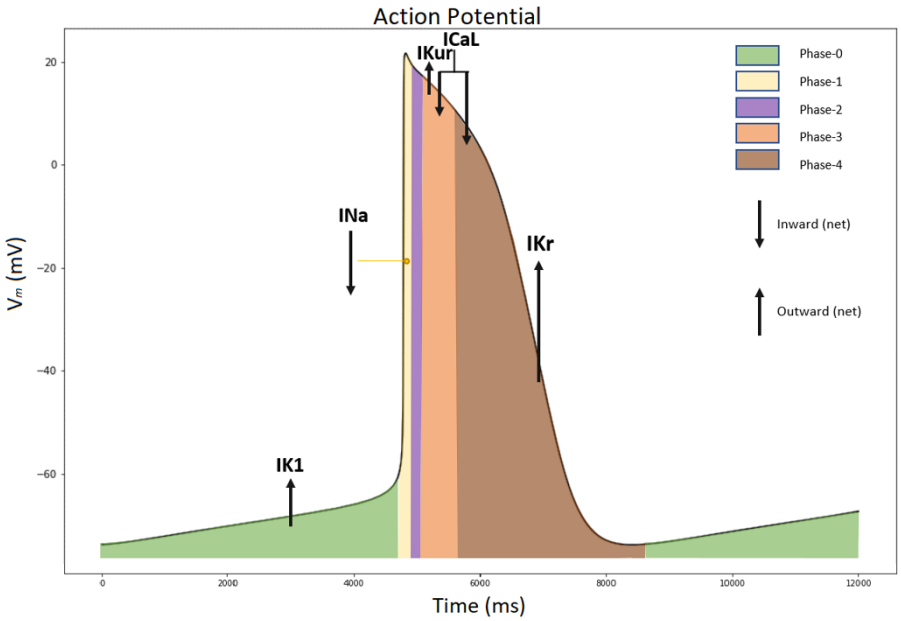

Figure 1. A typical action potential of an hiPSC-CM showing various phases of the action potential and main ionic currents active during each phase.

2 METHODS

2.1 LSTM Model

The LSTM model developed by Hochreiter et al. (Hochreiter & Schmidhuber, 1997) solved the vanishing gradient problem of RNNs that improved the long-term memory of the network. In our design, the AP time series information is stored in more than 1000 discrete time steps using a cell state (memory cell). The cell state runs for an entire time step and works as a bridge with the ability to add or remove information in the cell state, carefully managed by structures called gates. There are 3 different gates in an LSTM cell (see Figure 2): forget gate (f_t), input gate (i_t), and output gate (o_t). The output of an LSTM cell is the hidden state (h_t) which is used as an additional input for the next cell.

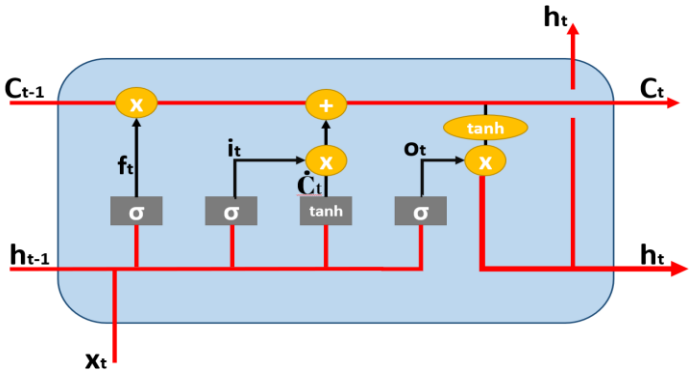

Figure 2: The LSTM block diagram.

The forget gate has a sigmoid activation function (σ) which passes information from the current input (x_t) and the prior hidden state (h_{t-1}) as given below. When the output value is close to 0, it implies forget, and when it is close to 1, it signifies keep.

$$f_t = \sigma\left(W_f \cdot [h_{t-1}, x_t] + b_f\right) \tag{1}$$

where *t* is timestep, W_f is a weight matrix of the forget gate, current input (x_t) and the prior hidden state (h_{t-1}) and b_f is the connection bias at *t*.

In the input gate, a second sigmoid function also receives the current state (x_t) and the previously hidden state (h_{t-1}). The values are changed from 0 (not important) to 1 (important). Next, the x_t and h_{t-1}will pass to a tanh operator and create a vector ($\check{C}_t$) with values between -1 and 1. The output values for sigmoid and tanh functions are suitable for point-by-point multiplication as shown below.

$$i_t = \sigma\left(W_i \cdot [h_{t-1}, x_t] + b_i\right) \tag{2}$$

$$\check{C}_t = \tanh\left(W_c \cdot [h_{t-1}, x_t] + b_c\right) \tag{3}$$

Where b_i is the bias vector, $\check{C}_t$ is the value generated by tanh, W_c is the weight matrix of tanh, and b_c is bias vector at t.

The cell state is generated by three steps. First, through the multiplication between the previous cell state (C_{t-1}), and the forget vector. If the result is 0, the values in the cell state will be discarded. Next, the network runs point-by-point addition on the output value of the input vector (i_t), giving the network a new cell state (C_t). In the last step, the output gate determines the value of the next hidden state. A third sigmoid function receives the current state (x_t) and the previously hidden state (h_{t-1}). The new cell state (C_t) passes through a tanh function. These two values are then multiplied point-by-point. The network selects which information the hidden state should store based on the final value. Prediction is based on this hidden state.

$$o_t = \sigma\left(W_o \cdot [h_{t-1}, x_t] + b_{o)}\right. \tag{4}$$

$$h_t = O_t * tanh\,(C_t) \quad (5)$$

Where h_t is the next hidden value, and (C_t) the next value for the cell state. Finally, the new cell state and hidden state are then passed forward to the next time step.

Multiple LSTMs can be stacked in a hierarchical fashion to build the features at the lower layers that will disentangle the factors of variations in the input data and then combine these representations at the higher layers. In case of large or complex data, it is demonstrated that such deep architecture will generalize better than a shallow architecture due to a more compact representation. (Hermans and Schrauwen 2013; Längkvist, Karlsson and Loutfi 2014; Utgoff and Stracuzzi 2002).

2.2 The Proposed Network Architectures

Our proposed network architecture uses a combination of LSTM layers and fully connected dense layers. Two different networks were designed to compare their abilities to effectively reproduce the experimentally observed AP morphology of hiPSC-CMs. The first architecture, shown in Figure 3A, used two back-to-back LSTM layers followed by three fully-connected dense layers. This network will be referred to as LSTM2. The second architecture, shown in Figure 3B, was composed of three back-to-back LSTM layers, and three fully connected dense layers. This network will be referred to as LSTM3. Inputs to each network are the scaling factors of maximum conductance of five main ionic channels, I_{CaL}, I_{K1}, I_{Kr}, I_{Kur}, and I_{Na}.

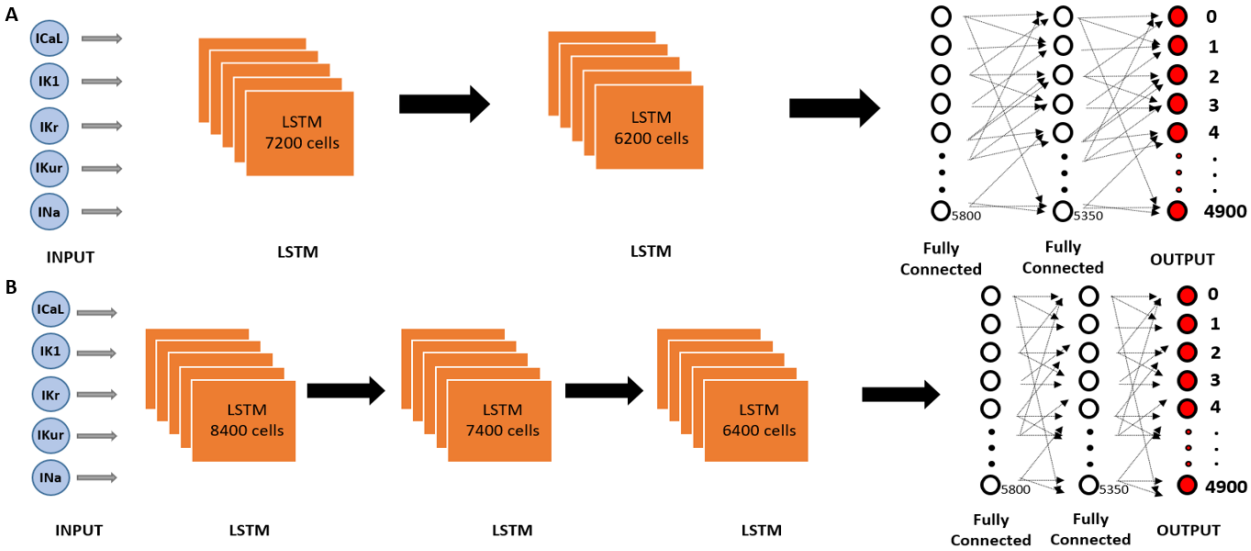

Figure 3: The proposed network designs for hiPSC-CM model. A) LSTM2 and B) LSTM3.

Each input value varies in the range of 0 to 2; where 2 represents a 200% scaling of corresponding current and 0 represents a complete block of the current. A value of 1 corresponds to the control value (no scaling) of the current conductance. For example, an input set of (1,1,1.4,1.4,1) corresponds to no scaling of I_{CaL} and I_{K1}, 40% increase in both I_{Kr} and I_{Kur}, and no scaling of I_{Na} conductance. The output of the network is the time series instances of the V_m values corresponding to the spontaneous APs in hiPSC-CMs. In each LSTM layer, the inputs at time *t*, $\boldsymbol{X}_t$, along with the previous hidden state $h^1{}_{t-1}$ (the superscript refers to the first LSTM) are used to compute the hidden state at time *t*, $h^1{}_t$,which is used in the next time step and is also supplied to the second LSTM block. The second LSTM uses the hidden state $h^1{}_t$ along with the previous hidden state $h^2{}_{t-1}$ to compute $h^2{}_t$, that is subsequently used in the next time step and as an input to the third LSTM block (in case of LSTM3). The benefit of such stacked architecture is that each layer can process a part of the desired task and subsequently pass it on to the next layer while constructing the long-term dependencies in a multivariate time series. Another advantage of this arrangement is that it allows the hidden states at each level to operate at different timescales (Fortin et al., 2012, Sagheer and Kotb, 2019).

The output of the last LSTM is further processed by three layers of a fully-connected network to simultaneously output all time points in the AP sequence.

The models were implemented and trained using TensorFlow and Keras library in a CPU environment. The training used Mean Square Error (MSE) loss function and Adam optimizer for adaptive learning rates (Goodfellow et al., 2016). The batch size was chosen to be 12. The number of final training epochs was automatically determined based on early stopping method.

2.3 Generation of Data

Training and testing data were created by simulating the original Akwaboah et al. model (Akwaboah et al., 2021). We chose the Akwaboah model because it is the most recent physiologically detailed model that is capable of reproducing experimentally observed electrophysiological behavior in hiPSC-CMs. The model has been extensively validated based on experimentally recorded AP data in hiPSC-CMs and can uniquely simulate the effects of atria-specific drugs and parasympathetic stimulation (Akwaboah et al., 2021). The maximum channel conductance values of $I_{CaL,}$ I_{K1}, $I_{Kr,}$ I_{Kur}, and I_{Na} currents were scaled in the range of 0% (complete block) to 200% (100% enhancement) in steps of 20%. Simulations were performed by manipulating single current conductances as well as combinations of changing multiple current conductances in each run, which produced a total of 341 simulations. However, some current combinations failed to generate an AP (e.g. I_{Na} conductance reduced by more than 50%) (Akwaboah et al., 2021). Such non-physiological current scaling combinations were removed from the training/testing data which resulted into a final dataset consisting of 252 unique simulations. Each simulation was run for a duration of 5000 ms with a time step of 0.05 ms, generating a total of 100,000 time points per simulation. To keep the computations tractable, each AP time series was split into smaller segments each consisting of 12000 time points. Each data sample was adjusted to contain a complete AP signal as shown in Figure 4. Next, the data was resampled using a Fourier method in SciPy library to 5000 time points per sample. Lastly, we deleted the first 50 and last 50 points due to susceptibility of noise. In all, the processed dataset consisted of 971 samples with 4900 time points each. The data was randomly divided into 80% for training and the remaining 20% for testing. The test data was also used for validation.

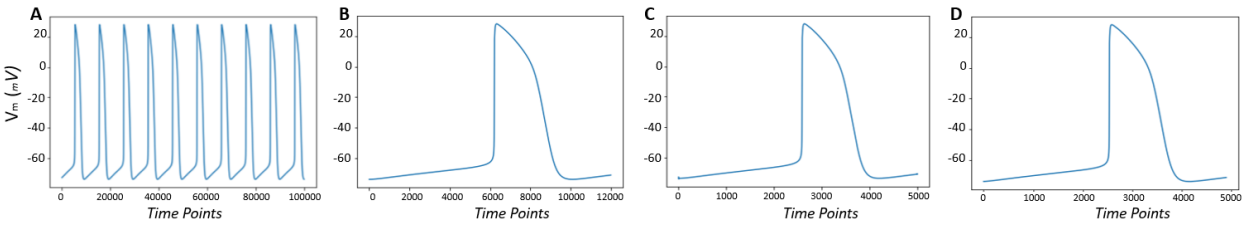

Figure 4: Downsampling of AP training data. A) Original AP time series containing 100,000 time points. B) A sample of the derived data segment. C) The AP data after downsampling. D) Final data sample with 4900 time points.

2.4 Postprocessing and Performance Metric

Our goal was to create a model capable of replicating the shape of an AP, automaticity and the values of AP durations at 50%, 75% and 90% of the maximum amplitude (APD_{50}, APD_{75}, and APD_{90}, respectively) using only the values of the current conductance scaling.

To counteract noise in the model output, we applied a 1-dimensional Gaussian filter using SciPy library.

$$g_\sigma(x) = \frac{1}{\sqrt{2\pi}\sigma} \exp\left(-\frac{x^2}{2\sigma^2}\right) \tag{6}$$

Where σ is the standard deviation.

As mentioned before, we used the Mean Square Error loss to penalize the weights during the training which is computed by:

$$MSE = \frac{1}{n}\sum_{i=1}^{n}(y_i - \hat{y}_i)^2 \quad (7)$$

Where y is the set of observed values, $\hat{y}$ is the set of predicted values and *n* is the number of data points.

To compare our results with the true data (simulated by Akwaboah model) we used mean absolute percentage error (MAPE) which is calculated by:

$$MAPE = \frac{100}{n}\sum\left|\frac{y-\hat{y}}{y}\right| \quad (8)$$

3 RESULTS AND DISCUSSION

Table 1 lists the two performance metrics, MSE and MAPE, for the models' outputs compared with the Akwaboah et al. model (Akwaboah et al., 2021). MSE represents the overall accuracy of the model output, while the MAPE measures the difference between the predicted and actual values of APD_{50}, APD_{75}, APD_{90} and APD_{all}. APD_{all} represents the average accuracy between all APD measurements (APD_{50}, APD_{75} and APD_{90}). The Gaussian σ values for smoothing out the predicted signal were varied between 1 and 8 in steps of 0.1. The best values of σ were found to be 2.2 for LSTM2, and 7.6 for LSTM3 models. Higher σ values produced distortions in the steep AP regions such as the upstroke (Phase 1-2) and maximum AP amplitude. It is evident from Table 1 that the LSTM3 model exhibits a better accuracy than the LSTM2 model due to the additional LSTM layer which improves its capacity to learn more complex temporal data patterns. In fact, both models were able to reliably produce AP morphologies of hiPSC-CMs (see Figure 5). The AP shape morphology and AP durations produced by our models match accurately with the experimentally recorded APs in hiPSC-CMs reported by Akwaboah et al. (Akwaboah et al., 2021). The training/validation process utilized the early stopping mechanism with zero patience. As observed from the table, the LSTM3 model required fewer epochs to converge than LSTM2. However, time per epoch was significantly higher due to the additional LSTM layer. The model execution time did not differ significantly between the two models.

Table 1: Performance Comparison of the AP Models.

Model	APD_{50} (MAPE)	APD_{75} (MAPE)	APD_{90} (MAPE)	APD_{all} (MAPE)	Loss Evaluate for the model (MSE)	No. Epoch / Time per Epoch(S)	Execute Time
LSTM2 σ = 2.2	2.331%	1.91%	2.268%	2.17%	14.748	923/150s	72.5 ms
LSTM3 σ = 7.6	1.323%	0.92 %	0.823%	1.022%	14.803	834/380s	80 ms

Figure 5 shows representative examples of the AP signals produced by the LSTM models for various scaling of ionic currents. The predictions of the LSTM3 model were smoother than those of the LSTM2 model. However, in both models some noise was observed during the AP plateau (Phase 2-3) and the diastolic interval (Phase 0) despite Gaussian smoothing. More importantly, the models were able to reproduce the experimentally observed behavior in cardiac myocytes (Ma et al., 2011) such as: 1) prolongation of AP when I_{Kr} or I_{Kur} are blocked and shortening of AP when I_{Kr} or I_{Kur} are enhanced, 2) shortening of AP plateau when I_{CaL} was blocked and prolongation when I_{CaL} was enhanced, 3) depolarization of maximum diastolic potential when $I_{K1}$was blocked and hyperpolarization when I_{K1} was enhanced.

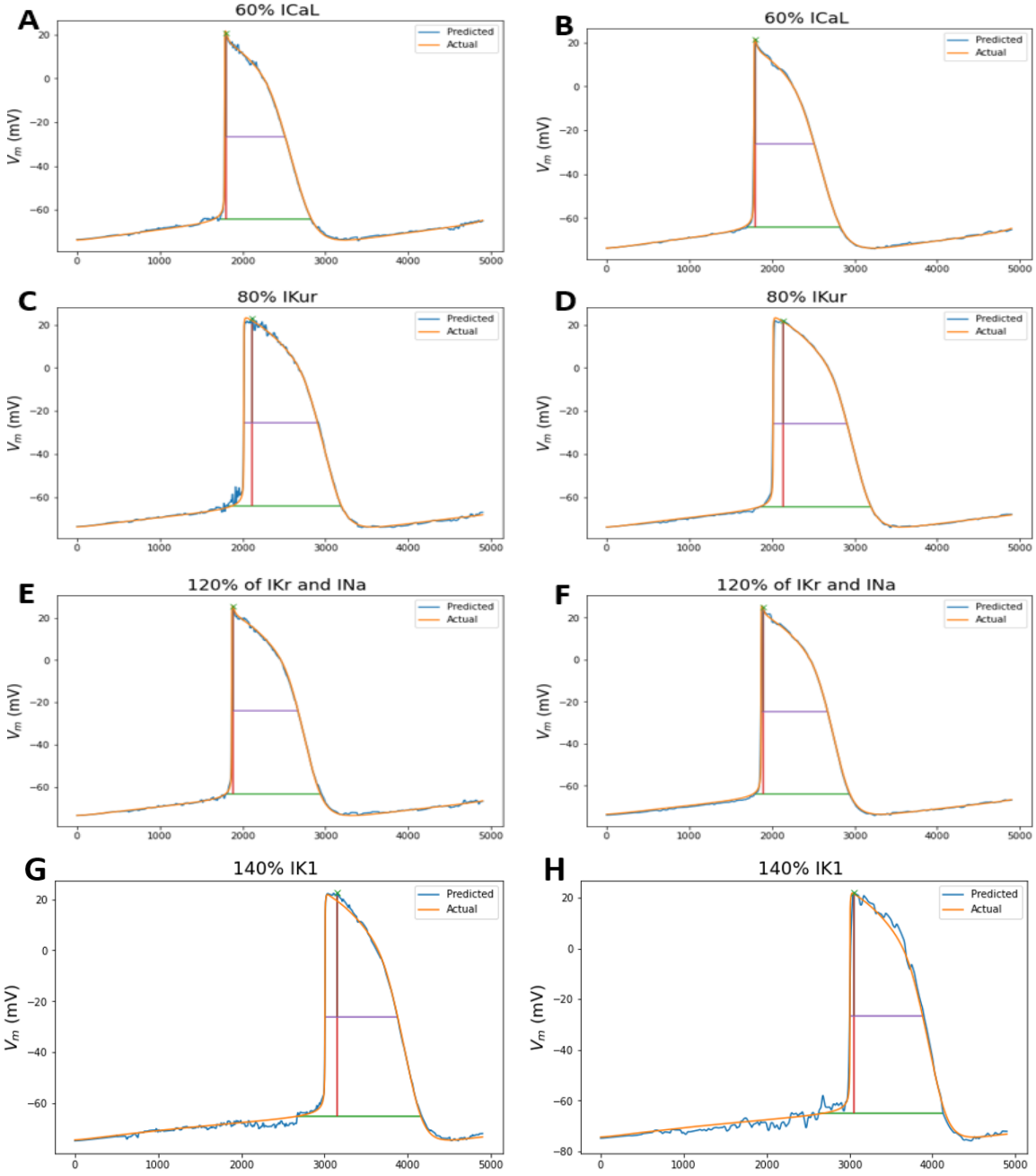

Figure 5: Sample AP traces produced by LSTM2 (left column) and LSTM3 (right column) models overlayed with true traces from Akwaboah model for various combinations of current conductance. The APD_{50} and APD_{90} measurements are shown by the purple and green lines, respectively. The green x-mark indicates the peak voltage amplitude, and the vertical red line represents the time instance corresponding to the maximum AP amplitude.

Figure 6 shows a detailed comparative sensitivity analysis of the LSTM models (Panels B and C) and that of the original Akwaboah model (Panel A) for the five main ionic currents and their effects on APD parameters. The figure shows color-coded correlation coefficients corresponding to the relation between the currents and AP durations. The figure shows a strong positive correlation coefficient between APD_{50} and I_{CaL}, which indicates that an increase in I_{CaL} causes an increase in APD_{50}. I_{Kr} and I_{Kur}, on the other hand, show a strong negative correlation with APD_{90} and APD_{75}. I_{K1} shows an almost neutral correlation with

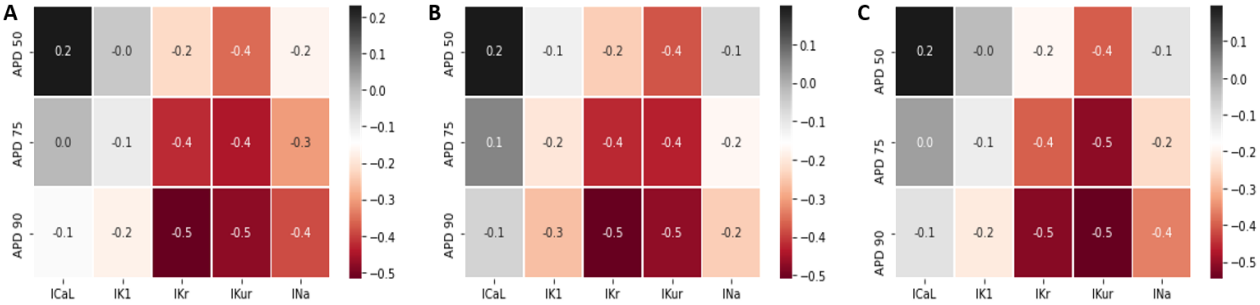

Figure 6: Sensitivity analysis in A) original Akwaboah, B) LSTM2 and C) LSTM3 models to study the effects of variations $I_{CaL,}$ I_{K1}, $I_{Kr,}$ I_{Kur}, and I_{Na} on the APD parameters.

APD. These results demonstrate that our LSTM models can faithfully produce the biophysical effects of ionic channel variations just as good as the detailed models. These analyses are important because they show that our models can be utilized to study the effects of various anti-arrhythmia drugs (Paci et al., 2020) such as E4031 and Dofetilide (potassium channel blockers), Diltiazem and Verapamil (calcium channel blockers), and flecainide (sodium channel blocker). Our models are also useful in studying arrhythmia mechanisms in inherited cardiomyopathies such as long/short QT syndrome (LQTS/SQTS), catecholaminergic polymorphic ventricular tachycardia (CPVT) and Brugada syndrome (Vaidyanathan et al., 2016).

This study demonstrates the feasibility of creating physiologically realistic predictive models using deep learning networks. The prediction capability of models can be further improved through continued fine-tuning using newer data based on advanced experimental investigations. The AP in excitable cells is an all-or-nothing phenomenon, i.e. when elicited, it goes through all phases (Phase 0 through Phase 4) and cannot be aborted midway. Therefore, we trained our models to output an entire hiPSC-CM AP sequence while preserving their ability to produce spontaneous automaticity. Our approach also enabled us to predict the physiological effects of AP prolongation/shortening and alterations in spontaneous firing rate (i.e. automaticity) in presence of partial or complete blockade of constituent ionic channels. Further investigations are needed to improve the training convergence of the models via advanced hyperparameter optimization techniques and improving the prediction time which may make them more attractive for in silico clinical trials.

4 CONCLUSION

Over the years, the applications for deep learning have increased exponentially, and time series is no exception. The LSTM's ability to find and keep patterns over many time steps is crucial for applications in non-linear time series, and the success of recent implementations have proven its importance. In this study, LSTM-based models were developed to describe the biophysical response of human induced pluripotent stem cell-derived cardiomyocytes. The models were trained with data from alterations in five main ionic current components that contribute to the action potentials in these cells. The model with 3 cascaded LSTM layers achieved an overall MSE of 14.803 and the action potential morphology was reproduced with accuracy close to 99%. These models were able to faithfully reproduce experimentally observed behaviors of ion channel blocks and drug interactions in cardiomyocytes. Further study should involve creating further finetuned models with the capacity to manipulate more currents, stimulus conditions, and refractory periods.

REFERENCS

Akwaboah, A. D., Tsevi, B., Yamlome, P., Treat, J. A., Brucal-Hallare, M., Cordeiro, J. M., & Deo, M. (2021). An in silico hiPSC-Derived Cardiomyocyte Model Built With Genetic Algorithm. *Frontiers in Physiology*, *12*. https://doi.org/10.3389/fphys.2021.675867

Colatsky, T., Fermini, B., Gintant, G., Pierson, J. B., Sager, P., Sekino, Y., Strauss, D. G., & Stockbridge, N. (2016). The Comprehensive in Vitro Proarrhythmia Assay (CiPA) initiative — Update on progress. *Journal of Pharmacological and Toxicological Methods*, *81*, 15–20. https://doi.org/10.1016/j.vascn.2016.06.002

Hermans, M. and Schrauwen, B., 2013. Training and Analysing Deep Recurrent Neural Networks. *Advances in Neural Information Processing Systems 26*, (NIPS 1), pp.190-198.

Längkvist, M., Karlsson, L. and Loutfi, A., 2014. A review of unsupervised feature learning and deep learning for time-series modeling. *Pattern Recognition Letters*, 42, pp.11-24.

Utgoff, P. and Stracuzzi, D., 2002. Many-Layered Learning. *Neural Computation*, 14(10), pp.2497-2529.

Sagheer, A. and Kotb, M., 2019. Time series forecasting of petroleum production using deep LSTM recurrent networks. *Neurocomputing*, 323, pp.203-213.

Fortin, F. A., De Rainville, F. M., Gardner, M. A. G., Parizeau, M., & Gagné, C. (2012). DEAP: Evolutionary algorithms made easy. *The Journal of Machine Learning Research*, *13*(1), 2171-2175.

Han, Z., Zhao, J., Leung, H., Ma, K. F., & Wang, W. (2021). A Review of Deep Learning Models for Time Series Prediction. In *IEEE Sensors Journal* (Vol. 21, Issue 6). https://doi.org/10.1109/JSEN.2019.2923982

Hochreiter, S., & Schmidhuber, J. (1997). Long Short-Term Memory. *Neural Computation*, *9*(8). https://doi.org/10.1162/neco.1997.9.8.1735

Ma, J., Guo, L., Fiene, S. J., Anson, B. D., Thomson, J. A., Kamp, T. J., Kolaja, K. L., Swanson, B. J., & January, C. T. (2011). High purity human-induced pluripotent stem cell-derived cardiomyocytes: Electrophysiological properties of action potentials and ionic currents. *American Journal of Physiology - Heart and Circulatory Physiology*, *301*(5), 2006–2017. https://doi.org/10.1152/ajpheart.00694.2011

Moretti, A., Bellin, M., Welling, A., Jung, C. B., Lam, J. T., Bott-Flügel, L., Dorn, T., Goedel, A., Höhnke, C., Hofmann, F., & others. (2010). Patient-specific induced pluripotent stem-cell models for long-QT syndrome. *New England Journal of Medicine*, *363*(15), 1397–1409.

Paci, M., Passini, E., Klimas, A., Severi, S., Hyttinen, J., Rodriguez, B., & Entcheva, E. (2020). All-Optical Electrophysiology Refines Populations of In Silico Human iPSC-CMs for Drug Evaluation. *Biophysical Journal*, *118*(10), 2596–2611. https://doi.org/10.1016/j.bpj.2020.03.018

Pascanu, R., Gulcehre, C., Cho, K., & Bengio, Y. (2014). How to construct deep recurrent neural networks. *2nd International Conference on Learning Representations, ICLR 2014 - Conference Track Proceedings*.

Pascanu, R., Mikolov, T., & Bengio, Y. (2013). On the difficulty of training recurrent neural networks. *30th International Conference on Machine Learning, ICML 2013*, *PART 3*.

Peter, G., & Matskevichus, M. (2019). Hyperparameters Tuning for Machine Learning Models for Time Series Forecasting. *2019 6th International Conference on Social Networks Analysis, Management and Security, SNAMS 2019*. https://doi.org/10.1109/SNAMS.2019.8931860

Vaidyanathan, R., Markandeya, Y. S., Kamp, T. J., Makielski, J. C., January, C. T., & Eckhardt, L. L. (2016). IK1-enhanced human-induced pluripotent stem cell-derived cardiomyocytes: An improved cardiomyocyte model to investigate inherited arrhythmia syndromes. *American Journal of Physiology - Heart and Circulatory Physiology*, *310*(11), H1611–H1621. https://doi.org/10.1152/ajpheart.00481.2015

Weerakody, P. B., Wong, K. W., Wang, G., & Ela, W. (2021). A review of irregular time series data handling with gated recurrent neural networks. *Neurocomputing*, *441*. https://doi.org/10.1016/j.neucom.2021.02.046

AUTHOR BIOGRAPHIES

BRUNA SILVEIRA GONCALVES is a Graduate Research Assistant at Norfolk State University. She is currently enrolled in the Master of Science in Electronics Engineering program. Her research interests are simulation modeling, especially in healthcare. Her email address is b.s.goncalves98@gmail.com.

MAKARAND DEO is an Associate Professor in the Department of Engineering at Norfolk State University, Norfolk, VA. His research interests include multiscale modeling and simulation of cardiac electrophysiology and biosensing systems. His email address is mdeo@nsu.edu.